Molecular Force Balance Measurements Reveal that Double-Stranded DNA Unbinds Under Force in Rate-Dependent Pathways

Christian H. Albrecht,* Gregor Neuert,† Robert A. Lugmaier,* and Hermann E. Gaub*
*Applied Physics and Center for NanoScience, Ludwig-Maximilians-Universität München, 80799 Munich, Germany; and †Massachusetts Institute of Technology, Department of Physics, Cambridge, Massachusetts 02139

ABSTRACT Strand separation of double-stranded DNA is a crucial step for essential cellular processes such as recombination and transcription. By means of a molecular force balance, we have analyzed the impact of different pulling directions and different force-loading rates on the unbinding process of short double-stranded DNA. At loading rates above 9×10^5 pN/s, we found a marked difference in rupture probability for pulling the duplex in 3′-3′ direction compared to a 5′-5′ direction, indicating different unbinding pathways. We propose a mechanism by which unbinding at low loading rates is dominated by nondirectional thermal fluctuations, whereas mechanical properties of the DNA become more important at high loading rates and reveal the asymmetry of the phosphoribose backbone. Our model explains the difference of 3′-3′ and 5′-5′ unbinding as a kinetic process, where the loading rate exceeds the relaxation time of DNA melting bubbles.

INTRODUCTION

Conversion of double-stranded DNA (dsDNA) into single strands is crucial for essential cellular processes such as recombination, replication, and transcription. Molecular machines have evolved different mechanisms, depending on their physical functions, to separate the two strands. In RecA-assisted recombination, for example, the helix is enclosed in a narrow tunnel where it is stretched, unwound, and subsequently denatured (1). In contrast, RNA polymerase forms a transcription bubble that moves along the DNA template while RNA is polymerized. As for any other molecular machine, two basic mechanisms have been discussed in terms of the opening of DNA during transcription: 1), the power stroke, where the hydrolysis of the triphosphates is efficiently converted into mechanical work; and 2), the Brownian ratchet, where the process mainly is powered by thermal noise while chemical energy predominantly is used to rectify those fluctuations (2). Interestingly DNA separation by means of force probe instruments has been discussed in a quite similar way. Again, one discrete ''mechanical'' and one fuzzy ''Brownian'' model have been put forward to describe the unbinding reaction yet without definitive answers. In our study, we probed short dsDNA at different ends and at different speed by means of a molecular force balance. This method revealed previously unknown mechanical properties of the DNA helix that provide new insights into the unbinding mechanism of DNA.

A molecular force balance measures differences in the unbinding probability under force by direct comparison of a sample bond (Fig. 1, *red*) to a reference bond (Fig. 1, *blue*). A large number of such balances are attached at their opposing ends between a glass slide and a silicone stamp and probed in parallel. On separation of stamp and slide, the polymeric spacers are gradually stretched, and the force builds up in the balances until either the reference bond or the sample bond fails, depending on which one has the higher bond strength (Fig. 1). As a consequence, the fluorescent label attached to the middle part of the balances will be found either on the stamp or on the glass surface. The difference in bond strength of the molecular complexes, therefore, can be quantified by measuring the fluorescence on both sides and provides the survival probability Φ_S of the sample bond (3,4). Due to the high sensitivity of this differential measurement principle, we could detect minute differences in binding force, as demonstrated for the discrimination between different kinds of single mismatches in 30 bp DNA (4,5). In addition, we established the concept of ''dynamic'' differential force measurements, where the duplexes are loaded with different rates. Compared to ''static'' measurements at constant velocity, dynamic studies are suited to map the energy landscape at many points, thereby revealing kinetic unbinding barriers (6–9).

Single-molecule force spectroscopy studies have demonstrated that only moderate forces in the piconewton range are required to disrupt receptor-ligand complexes, such as biotin-streptavidin, or to separate the strands in dsDNA, as long as only moderate loading rates are applied to the bond. This is because thermal fluctuations contribute to the unbinding reaction (10). Accordingly, a linear correlation between the logarithm of the loading rate and the rupture force has been measured for the unbinding of different short DNA duplexes (7). By means of a molecular force balance, we demonstrate that short dsDNA shows a nonlinear force response when a critical loading rate of $\sim 9 \times 10^5$ pN/s and a rupture force of $\sim$68 pN are exceeded, indicating a change in the unbinding pathway. This effect is caused by an asymmetry between 5′-5′ and 3′-3′ pulling direction that becomes significant when DNA is probed at a kinetic regime where mechanics dominates

Submitted November 8, 2007, and accepted for publication January 24, 2008.
Address reprint requests to Hermann E. Gaub, E-mail: gaub@lmu.de.
Editor: Jonathan B. Chaires.

0006-3495/08/06/4766/09 $2.00
doi: 10.1529/biophysj.107.125427

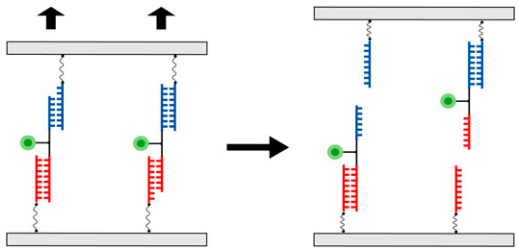

FIGURE 1 Differential force measurement with a molecular balance. Two force balances consisting of a reference duplex (*blue*) linked to a sample duplex (*red*) are immobilized and probed between two surfaces. Whereas the reference duplex is recessed in the left balance, the sample duplex is the shorter one in the right balance. The fluorescent label attached to the middle part of the balances either ends up on the upper surface, when the bond strength of the reference duplex is higher than that of the sample duplex, or on the bottom, when the bond strength of the reference duplex is lower than that of the sample duplex.

thermal fluctuations. We discuss this behavior by reconciling two opposing models put forward to explain the transition state of DNA unbinding (''force-induced melting'' as a hypothesis for the B- to the S-form transition) (11–13) and overstretching (''S-form'' stretched conformations with intact base pairing) (14,15).

MATERIAL AND METHODS

The differential force assay

In contrast to force probe techniques, in which individual molecules are loaded by means of a microscopic transducer, the differential measurement was performed simultaneously on a macroscopic number of balances ($\sim 10^9$) by probing the molecular bridges that had formed over a large area of ~ 1 mm^2 between a silicone stamp and a glass slide. To assemble the balances, amino-modified oligonucleotides were immobilized on an aldehyde-activated glass slide. Oligonucleotides labeled with Cy3 fluorophore then were hybridized to the aminooligonucleotides, thus forming a sample duplex. Subsequently, oligonucleotides labeled with biotin at the 5′-terminus were hybridized to the Cy3-oligonucleotide thereby forming a reference duplex. (Oligonucleotides used in this study were purchased from IBA, Goettingen, Germany.) The structure of the balance used for this study is depicted in Table 1, which shows one force balance in standard orientation (top), one in upside-down orientation (middle), and one with restored symmetry, where both duplexes were probed in 5′-5′ direction (bottom).

Coupling of the balances to the silicone stamp was facilitated by streptavidin-biotin interaction as depicted in Fig. 2 *c*. The silicone stamp comprised 16 protruding pads, each with a diameter of 1.1 mm. Each pad was brought into contact with a spot of force balances on the slide (Fig. 2 *a*). The top of each pad was structured by a micropattern of rectangular contact areas that were elevated by 5μm (Fig. 2 *b*). When the stamp was moved closer to the slide, each of the rectangular areas made contact with it and coupled to multiple balances (represented by a single balance in Fig. 2 *c*). The trenches served as drainage channels. After coupling, the stamp was separated from the slide by means of a piezo actuator, thereby probing and rupturing the balances. This resulted in a distribution of the Cy3 labels between stamp and slide, which was read by a laser scanner (Fig. 2 *d*). Coupling of the balances to streptavidin and disruption of the balances were performed at 25°C in 1× SSC buffer (150 mM NaCl; pH 7.2). For further details about these methods, see Albrecht and colleagues (4).

To correct for those balances that had not coupled to the stamp, soluble streptavidin-AlexaFluor647 conjugate was bound to the free biotin residues on the slide, and the signal again was read by the scanner. The output of a differential force experiment, the survival probability of the sample duplex Φ_S, was calculated from four input parameters that were extracted from the two fluorescence scans, as depicted in Fig. 3. The remaining Cy3 intensity ($Cy3_{REM}$) was extracted from the rectangular prints in the green scan, where contact had been established between stamp and slide. $Cy3_{REM}$ corresponded to balances that had been probed and ruptured at the reference duplex as well as to balances that had not been coupled to the stamp, thereby causing an offset. The start Cy3 intensity ($Cy3_{START}$) that corresponded to the initial density of balances immobilized on the slide was extracted from the grid pattern in the green scan. If the coupling efficiency of the balances was 100%, then the survival probability of the sample bond would be $\Phi_S = Cy3_{REM}/Cy3_{START}$. However, both Cy3 variables first had to be corrected for the offset of balances that had not been coupled. The red scan, therefore, was analyzed in terms of the remaining biotin density ($AF647_{REM}$) and the start biotin density ($AF647_{START}$) (Fig. 3). The degree of coupling then corresponded to $AF647_{REM}/AF647_{START}$, and the offset was calculated as follows:

$$Cy3_{offset} = Cy3_{START} \cdot \frac{AF647_{REM}}{AF647_{START}}.$$

The survival probability of the sample duplex Φ_S was determined from the offset corrected $Cy3_{REM}$ normalized to the offset corrected $Cy3_{START}$ as follows:

TABLE 1 Molecular balances in standard orientation (top) upside-down orientation (middle), and with restored symmetry where both duplexes are probed in 5′-5′ direction (bottom)

Oligo dir.	Pulling dir.	Oligo No.	Sequence
3′-5′	**3′-3′**	134	<-NH2-10t-**CTGCAGGAATTCGATATCAAGCTTATCGAT**
5′-3′		118	**GACGTCCTTAAGCTATAGTTCGAATAGCTA**c-8t-Cy3-8t-cATCGATAAGCTTGATATCGAATTCCTGCAG
3′-5′	5′-5′	62	TAGCTATTCGAACTATAGCTTAAGGACGTC-10t-Bio->
5′-3′	5′-5′	124	<-NH2-10t-CTGCAGGAATTCGATATCAAGCTTATCGAT
3′-5′		118	GACGTCCTTAAGCTATAGTTCGAATAGCTAc-8t-Cy3-8t-c**ATCGATAAGCTTGATATCGAATTCCTGCAG**
5′-3′	**3′-3′**	125	**TAGCTATTCGAACTATAGCTTAAGGACGTC**-10t-Bio->
5′-3′	**5′-5′**	113	<-NH2-10t-**TAGCTATTCGAACTATAGCTTAAGGACGTC**
3′-3′		117	**ATCGATAAGCTTGATATCGAATTCCTGCAG**c-6t-Cy3t-sfb-sanh-8t-cATCGATAAGCTTGATATCGAATTCCTGCAG
3′-5′	5′-5′	123	TAGCTATTCGAACTATAGCTTAAGGACGTC-10t-Bio->

The sequences of the middle oligonucleotide of the rectified balance (bottom) were synthesized separately and then conjugated by SFB-aldehyde and SANH-hydrazine reagents (Merck, Darmstadt, Germany). Left = slide; right = stamp. Sample duplex (*bold*) and reference duplex (*normal*). Labels: NH2 = amino; Cy3 = Cyanin-3 fluor; Bio = biotin; 8t = poly-t-spacer. The force is applied along the arrows. The sequences of the middle oligonucleotide of the balance were synthesized separately and then conjugated by SFB-aldehyde and SANH-hydrazine reagents (Merck).

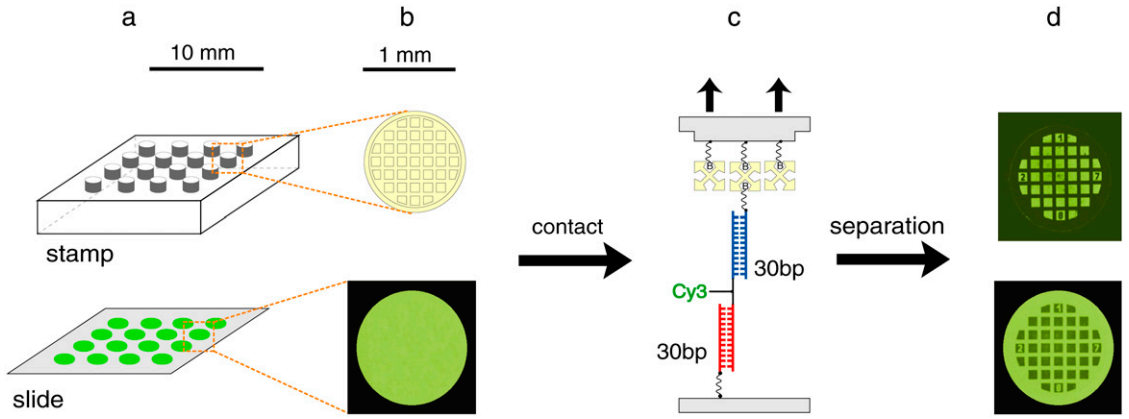

FIGURE 2 Contact and separation of stamp and slide. (*a*) Scheme of a silicone stamp having 16 contact pads and a glass slide having 16 spots of force balances. (*b*) A single pad with a microstructure of elevated rectangular contact areas covered with streptavidin (*yellow*) and a fluorescence image of a single spot (*green*). (*c*) Coupling of a single biotinylated force balance (representing a multitude of balances at one contact area) to streptavidin on the stamp. (*d*) Fluorescence image of stamp and spot after separation: The dark rectangular prints in the spot indicate where contact has been established and balances have coupled to the stamp.

$$\Phi s = \frac{Cy3_{\mathrm{REM}} - Cy3_{\mathrm{offset}}}{Cy3_{\mathrm{START}} - Cy3_{\mathrm{offset}}}.$$

Correction for coupling efficiency and normalization to $Cy3_{\mathrm{START}}$ were performed for all experimental data. For the images in Figs. 5 and 8, an average $Cy3_{\mathrm{offset}}$ was determined from all contact areas. For the plots in Fig. 6, the correction was calculated separately for the referring contact area.

Dynamic differential force assay

Due to the accumulative binding force of $\sim 10^9$ molecular balances at one contact area, a very strong interaction is created between stamp and slide. The stamp, therefore, is not separated immediately over the whole contact area; it deforms elastically instead and detaches in a propagating cleft from the rigid slide when pulled apart by the piezo actuator. This separation process commences at the edges of the rectangular contact areas and moves forward until complete separation (Fig. 4 *a*).

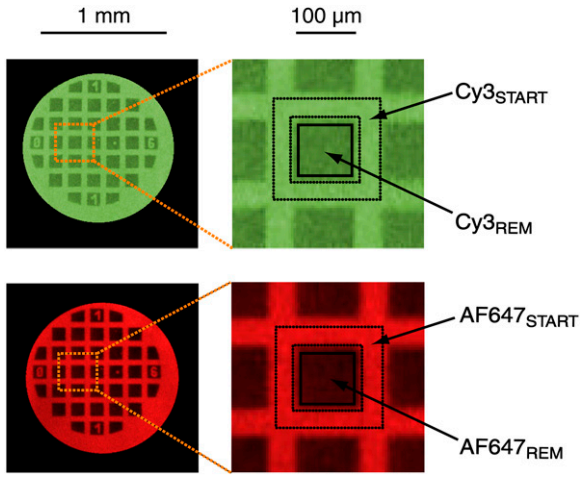

FIGURE 3 Two images of the same spot after separation. Dark squares correspond to the contact area where the balances have ruptured. Scans for Cy3 (*green*) and for streptavidin-AlexaFluor647 (*red*), which was bound to free biotins after scanning for Cy3. $Cy3_{\mathrm{START}}$ intensity and $AF647_{\mathrm{START}}$ intensity are derived from the area surrounded by the dashed lines. $Cy3_{\mathrm{REM}}$ intensity and $AF647_{\mathrm{REM}}$ intensity are derived from the area surrounded by the solid lines.

As long as the stamp is pulled apart by low velocities up to ~50 nm/s, the lateral speed of the cleft propagation is almost constant over all contact areas of the stamp. However at elevated piezo speeds, detachment does not keep pace with movement in the *z*-direction, and strain accumulates in the stamp. This tension leads to a nonlinear separation behavior; detachment occurs relatively slow at the edges of the contact areas but accelerates markedly toward the points where contact remains longest. As a consequence, a steep velocity gradient and a broad range of loading rates are accomplished over a single contact area. We used this effect for dynamic measurements and analyzed the velocity gradient by means of reflection interference contrast microscopy (RICM) in a manner comparable to the approach used by Leckband (16). For this purpose, we mounted the contact device on an inverted microscope (Axiomat; Zeiss, Goettingen, Germany) as depicted in Fig. 4 *a*. The contact interface of stamp and slide was illuminated by means of a xenon arc lamp, a neutral 50/50 beam splitter, and a 628/40-nm HC bandpass excitation filter (AHF Analysentechnik, Tuebingen, Germany) through a 10× Fluar objective (NA 0.5) (Zeiss). Separation was filmed at 500 frames/s with a high-speed camera (PCO 1200HS; PCO, Kehlheim, Germany). A single RICM frame of the whole stamp pad is depicted in Fig. 4 *a*; individual contact areas are shown in Fig. 4 *b*.

The effective separation velocities were derived by converting the lateral movement of the first and second interference maximum into separation distances in the *z*-direction, according to the method described by Wiegand et al. (17) and Rädler and Sackmann (18). This was done under the assumption that the geometry of the separation cleft in a first approximation (Fig. 4 *a*) is wedge-shaped, which was corroborated by finite element simulations not shown here. In Fig. 4 *b*, four frames from a high speed RICM movie are shown; they were analyzed along a region of interest with a width of three pixels (white line) by plotting an averaged intensity profile over the position on the slide (shown here for frames one and two). The first (L_1) and second (L_2) maximum next to the contact area were fitted with a Gaussian curve to determine their lateral position. The lateral velocity v_{L} of the peeling process was determined from a diagram on which the first maxima were plotted as a function of position and time. From the lateral distances (L_1 and L_2) and the heights of the interference maxima ($h_1 = 124 \pm 3$ nm and $h_2 = 362 \pm 5$ nm at a 628-nm wavelength), a conversion factor k was derived. This transformed the lateral peeling speed into a *z*-directional separation velocity via $v_z = k \times v_{\mathrm{L}}$ with $k = (h_2 - h_1)/(L_2 - L_1)$ (17). After a certain progress in separation, however, the first and second interference maximum around the

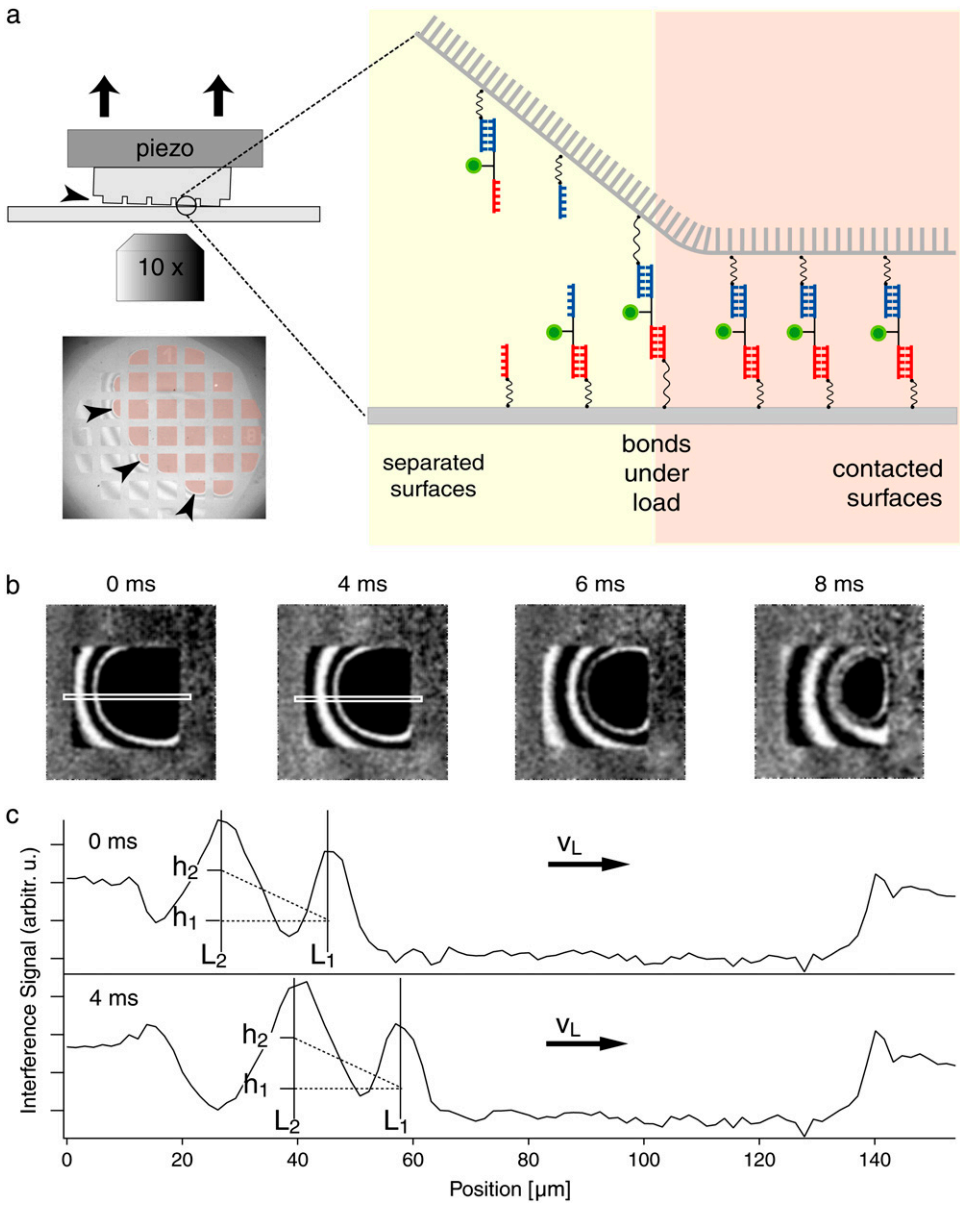

FIGURE 4 (*a*) Schematics and interference micrograph of slide-stamp separation driven by piezo movement. Slide-stamp contact areas (*light red*) are separated at the edge of the propagating cleft at which the balances are loaded and ruptured. The separation direction is indicated by black arrowheads. (*b*) RICM images show a single contact area at different times: 0 ms, 4 ms, 6 ms, and 8 ms. Each profile is measured along the white marking, which is perpendicular to the direction of movement of the bright interference rings (*images* on the *left side*). (*c*) RICM profile at the time $t_1 = 0$ ms (*upper section*) and at the time $t_2 = 4$ ms (*lower section*) showing the first and second interference maximum at the positions L_1 and L_2. Between the frames 0 ms and 4 ms, the two maxima move with a lateral velocity $v_L = 3.1 \times 10^3$ μm/s to the right. This corresponds to a stamp-slide separation velocity $v_Z = 40$ μm/s (see text for calculation). The heights of the stamp over the slide are referred as h_1 and h_2 for the first and second maximum.

contacted area started to merge and became indistinguishable. This effect indicates that the slope of the stamp reaches the limit of the vertical resolution at this point, which can be estimated from the difference in height between the first and the second maximum (238 nm) divided by the limit of the lateral resolution (2380 nm), which corresponds to two camera pixels. The resolution limit of the slope, therefore, is an angle of 5.7° (tangent = 0.1). Because the velocity could not be determined after that point, it was extrapolated with a linear fit function (see Fig. 6, *dotted line*).

To transform the velocity profile obtained through RICM analysis into a loading rate profile, a simulation based on atomic force microscopy measurements was performed. A standard force curve for stretching a polymeric polyethylene glycol linker, which connects the balances to the stamp, was calculated with a freely jointed chain model. We assumed that the polyethylene glycol linker consisted of 68 monomers and accounted fully for the overall spring constant of the system. The spring constant of the silicone is very high and so negligible; we used a spring constant of 1000 pN/nm for the transducer. According to the method described by Friedsam et al. (19), we calculated the probability distributions of rupture force $P(F)$ and loading rate $P(r)$ for every point in the separation velocity profile. Their maxima provide the most probable rupture force and the corresponding loading rate, which depends on the bond strength. We could do so because we had previously characterized the binding potential of a 30 bp DNA duplex by atomic force microscopy measurements. A potential width $\Delta x = 2.9$ nm and a natural dissociation rate $k_{off} = 4.4 \times 10^{-15}$ s^{-1} was found and taken for these calculations. The values are in good agreement with data obtained by other groups (7). The most probable loading rate that corresponds to each point in the measured velocity profile is plotted with the survival probability over the distance in Fig. 6.

RESULTS AND DISCUSSION

In Fig. 5, three experiments are depicted in which the same kind of force balance was investigated at different velocities and molecular orientations. Sections of DNA spots on the slides are shown where fluorescence intensity was corrected

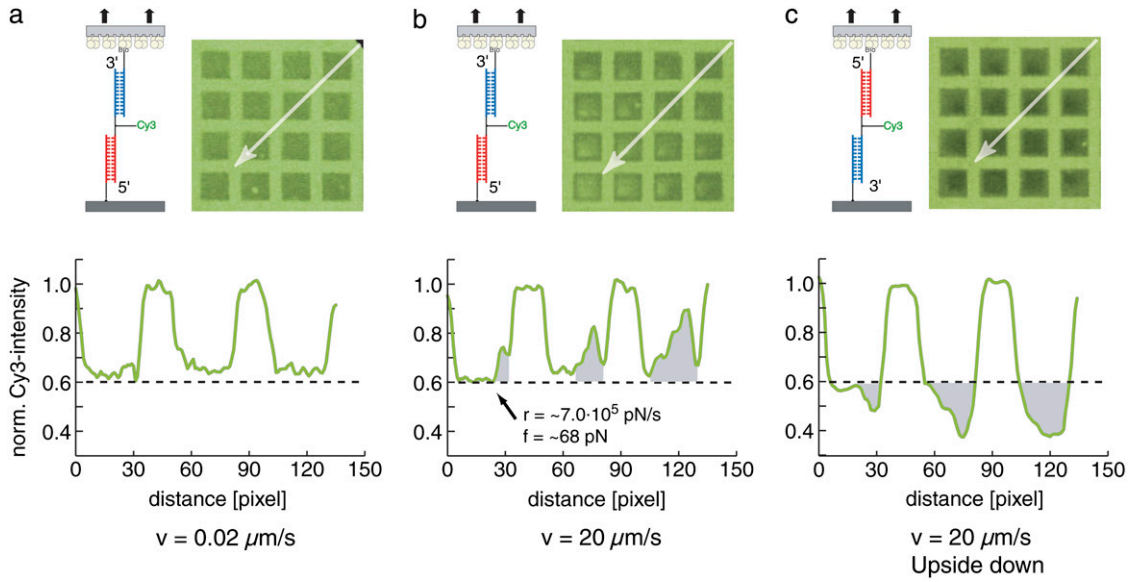

FIGURE 5 Normalized Cy3 intensity images where the contact areas correspond to Φ_S (survival probability of the sample duplex (*red*)). White selections in the images are plotted as normalized intensity over distance. Gray areas in the diagrams are specifying the nonlinear effect. (*a*) Molecular force balance probed at 0.02 μm/s: The curve sections between the peaks (Φ_S) are relatively flat. (*b*) Molecular force balance probed at 20 μm/s: Φ_S is increasing steeply in some contact areas. For the onset of the peaks, loading rate and rupture force were calculated (*black arrow*). (*c*) Molecular force balance turned upside-down and probed at 20 μm/s. Φ_S is steeply decreasing in some contact areas. Images were smoothed by a median filter.

for coupling efficiency and normalized to the start values (intensity of the grid). The area of contact between slide and stamp corresponds to the darker squares, where Cy3-labeled oligonucleotides were probed and removed from the slide. The normalized intensity of the squares corresponds to the survival probability Φ_S of the sample duplex. In Fig. 5 *a*, the stamp was pulled apart by a very low velocity of 0.02 μm/s. The profile (measured along the white arrow in the micrograph) shows normalized intensities between ~0.6 and 1. High values around 1 correlate with the grid structure in the micrograph, whereas the lower values originate from the rectangular contact areas and correspond to the survival probability of the sample duplex Φ_S. Apart from some noise, the Φ_S profile is relatively flat. For the experiment shown in Fig. 5 *b*, the stamp was removed a thousand times faster at 20 μm/s. Under these conditions, the stamp distorts on retraction, which results in even higher peak values for the separation velocities in the centers of the square. Although the graph again shows Φ_S values of ~1 for the grid, the centers of the squares exhibit large irregularities throughout the contact area where Φ_S increases abruptly and culminates in peaks of ~0.9.

To address the question of whether the correlation of high survival probabilities Φ_S and high velocity shown in Fig. 5 *b* is an intrinsic property of the molecular balance, it was probed in an upside-down orientation, also at 20 μm/s. In fact, a similar effect but with an inverted sign, as shown in Fig. 5 *c*, was the consequence. As expected, Φ_S dropped to minima of ~0.35 instead of causing high values as in the previous experiment. This finding unambiguously corroborates the assumption that the Φ_S maxima and minima in Fig. 5, *b* and *c*, reflect an increased stability of the sample duplex compared to the reference duplex at higher pulling velocities. It was thus desirable to determine the effective local pulling velocities, which apparently were different from the external velocity of piezo movement. As described above, contacting and separating stamp and slide was monitored by interference contrast microscopy. Inspection of the interference pattern supported the hypothesis of a dynamic separation process, starting with slow separation at the edges of the contact area and accelerating substantially toward the points where contact was maintained for the longest period of time. The velocity gradient was determined by RICM analysis along a section that crossed the nonlinear effect (Fig. 6, *white arrow*). Additionally, the loading rate profile and the force profile were calculated as described in the Materials and Methods section. Velocity and loading rate were plotted with the survival probability over the distance on the slide in Fig. 6 (see Fig. S1, Supplementary Material, Data S1, for force profile plotted with survival probability). Although a loading rate of 7×10^5 pN/s and a rupture force of ~68 pN was determined for the curve shown in Fig. 6 at the onset of the nonlinear effect, the average value was slightly higher. The average values as derived from six curves, each from a different contact area of the same spot, were as follows: $9.5 \times 10^5 \pm 1.6 \times 10^5$ pN/s of loading rate and 68.4 ± 0.3 pN of rupture force at 0.64 ± 0.01 of survival probability.

We concluded that the system obviously exhibits an asymmetry at high pulling velocities, despite both duplexes differing by only ~3% in Gibbs free energy when calculated with

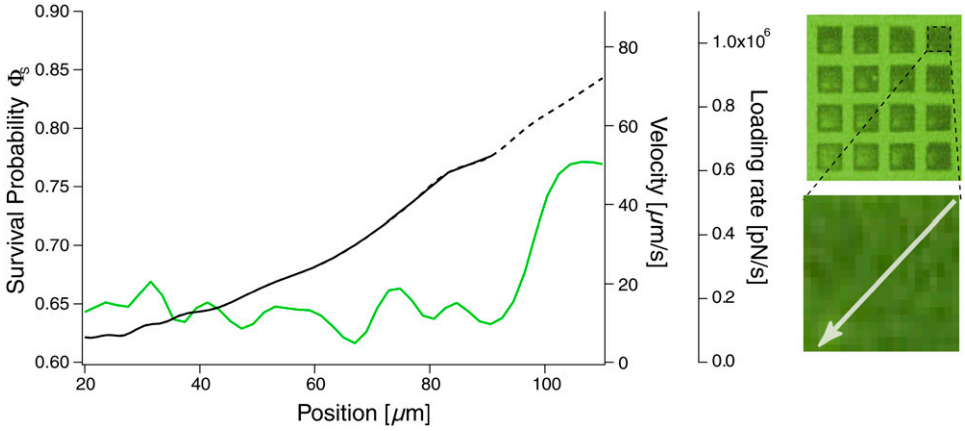

FIGURE 6 Upper right contact area of experiment in (Fig. 5 *b*). Survival probability of the sample duplex Φ_S was plotted over position on the slide (*green line*). Velocity and loading rate (*black line*) were determined as described above (*dotted black line*: extrapolated).

the nearest neighboring algorithm (20). This result was surprising because the balance should be insensitive to velocity changes due to its putative symmetry. To search for the break in the symmetry, we dissected the structure of the force balance as shown in Fig. 7. It became obvious that the assembly of the three oligonucleotides resulted in a lower duplex with 3′-3′ pulling direction and an upper duplex with 5′-5′ pulling direction. We concluded, therefore, that asymmetry in pulling geometry between the upper and lower duplex caused the nonlinear effect. To test this hypothesis, we designed a new balance with restored symmetry, (except for the chirality) in which both duplexes were probed in the same backbone direction (Fig. 7 *a*) (see Table 1 for design). As expected, the balance with restored symmetry exhibited no kinetic peculiarities, as shown in Fig. 7 *b*. In fact, the Φ_S profile stayed flat for pulling velocities between 0.02 and 20 μm/s and for loading rates as high as those depicted in Fig. 5 *b*.

We made another interesting discovery from various experiments in which balances were probed at 20 μm/s or higher. Fig. 8 shows an experiment in which the standard

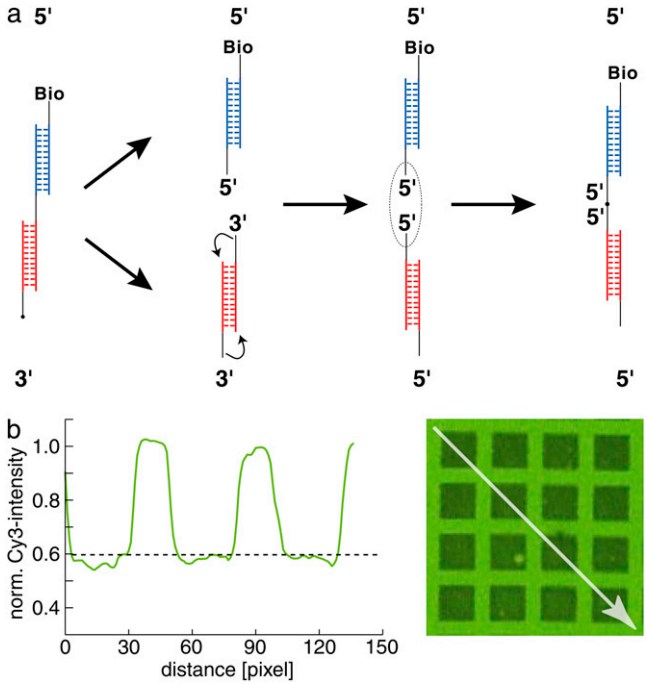

FIGURE 7 (*a*) Design of a fully symmetric balance. After dissecting the standard balance (*left*), it is evident that the sample duplex (*red*) is probed in 3′-3′ direction and the reference duplex (*blue*) in 5′-5′ direction. Conjugation of the duplexes at their 5′-termini results in a rectified balance, where both duplexes are probed in 5′-5′ direction. The plot refers to the white arrow in the micrograph. (*b*) The loading rate dependence observed for the standard balance (Fig. 5 *b*) was canceled out by the design with restored symmetry. The curve was smoothed by a median filter.

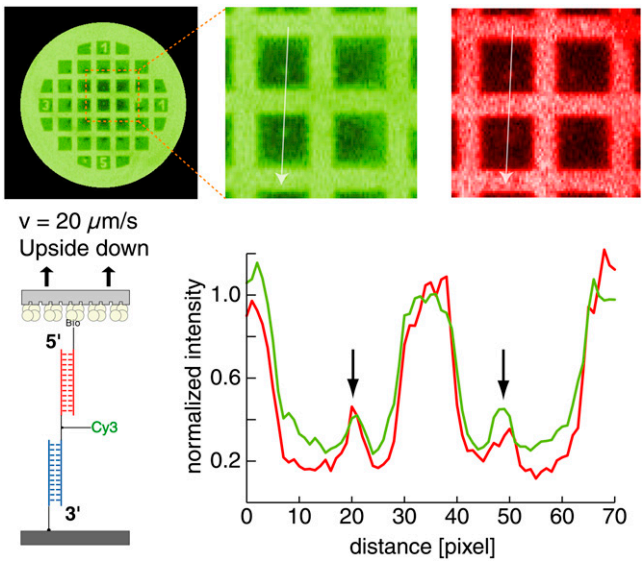

FIGURE 8 Experiment of an asymmetric standard balance in upside-down orientation pulled at 20 μm/s. Enlarged images of the contact area where the putative final contact points and show intensity peaks for Cy3 (*green*) and streptavidin-AlexaFluor647, which was bound to free biotins (*red*). The line plots, which are represented by the white arrows in the enlarged images, show a section through two contact areas and the putative last contact points where velocity and force-loading rate are assumed to be maximal (*black arrows* in the plot). Spikes in the Cy3 signal and AF647 signal indicate that bonds between biotin-oligonucleotide and streptavidin were ruptured at these points.

balance was immobilized in upside-down orientation comparable to that shown in Fig. 5 *c*. For the green images, the Cy3 signal was normalized to the start intensity. In Fig. 8, free biotins were labeled with soluble streptavidin-AlexaFluor647 conjugate after separation of stamp and slide, and the image again was normalized to the start intensity. In general, the Cy3 signal decreases to the center of the contact areas comparable to the spots depicted in Fig. 5 *c*. An additional effect, however, is evident in the middle of the central contact areas, where spikes of increased Cy3 intensity are visible in the enlarged images in the figure. Moreover, these spikes are also present in the AlexaFluor647 image at exactly the same location as evidenced by the line plots. At these locations, both DNA duplexes obviously are still intact, but biotinylated oligonucleotides were ruptured from the streptavidin on the stamp.

That different unbinding geometries of the same molecule could cause significant differences in rupture force most convincingly has been demonstrated by a comparison of DNA unzipping and shearing. Whereas the unzipping of a 16mer by pulling apart the 5′ and 3′ termini at one duplex end requires a force of only ~10 pN, for shearing in 5′-5′ direction ~37 pN has been determined at a loading rate of 24 pN/s (21). Comparable results have been obtained by force balance experiments, when those different unbinding geometries have been measured directly (3,4). Although diverging forces for unzipping and shearing DNA are very intuitive, this is not the case for the two possible shear directions 5′-5′ and 3′-3′, which generally are assumed to exhibit similar unbinding characteristics. To date, no disparity has been measured, and even sophisticated considerations of DNA melting under force do not provide an explanation for it (12). The only hint comes from simulations where different transition states have been proposed for polymeric DNA, namely a narrow fiber for 5′-5′ and an unwound ribbon for 3′-3′ pulling direction (Fig. 9 *d*) (14,15,22).

Fig. 5 *b* shows that the balance becomes asymmetric once a critical loading rate is exceeded. The effect was found to appear at a loading rate of $\sim 9 \times 10^5$ pN/s and a rupture force of ~68 pN and is due to a kinetic unbinding barrier comparable to those which have been reported for the biotin-streptavidin and hapten-antibody complexes (9,23). Our study demonstrates that the asymmetry occurs because of the difference in geometry of the 5′-5′ and 3′-3′ pulling direction and disappears when a balance with restored symmetry consisting of two 5′-5′ duplexes is used (Fig. 7). We assume that the so-called ''S-form'' transition states (14,15), which are structurally different for the two pulling directions (Fig. 9 *d*), are the origins of the asymmetry. Because this asymmetry only becomes apparent above a critical loading rate, however, another unbinding mechanism, which is insensitive to the pulling direction, must exist at lower loading rates. We assume that DNA bubbles are responsible for unbinding at low loading rates, according to the force-induced melting hypothesis (12). Because those thermal fluctuations are not

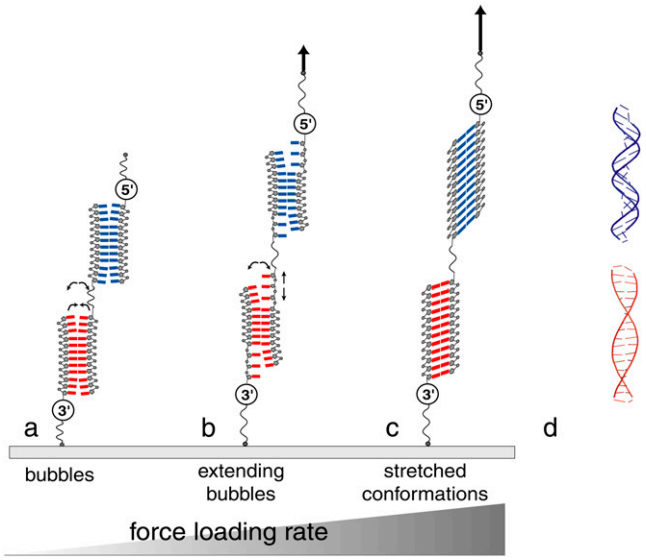

FIGURE 9 Model for the dominant transition state of DNA rupture dependent on pulling geometry and force-loading rate. (*a*) Unstretched B-DNA at zero force: Fluctuations are opening and closing the duplex at the ends (*curved arrows*). (*b*) At moderate loading rates, bubbles are growing because the applied strain hinders the closing reaction (*small vertical arrows*). (*c*) At loading rates higher than 9×10^5 pN/s, the duplexes are forced into stretched conformations with intact base pairing. (*d*) 5′-5′ and 3′-3′ pulling directions lead to different duplex structures (polyGC duplexes stretched 1.6 times (14,22)).

directed, they are suited to obscure most of the geometrical difference of unbinding in 5′-5′ and 3′-3′ direction. Hence, a distinction could be drawn between two regimes of unbinding: 1), a regime in quasiequilibrium at low loading rates where the reaction takes place assisted by thermal fluctuations, and 2), a kinetic regime at elevated loading rates where deformation is dominant over fluctuations and geometric properties of the helix are more meaningful. Altan-Bonnet and colleagues (24) have demonstrated that AT-rich sequences in a short duplex give rise to bubble-like fluctuations, which are characterized by a rate of $10^4 - 10^5$/s. We interpret this breathing rate of DNA as an attempt frequency ν_{off} for overcoming the potential well of the duplex bond. In combination with the observed force-loading rate $r \sim 9 \times 10^5$ pN/s at the onset of the kinetic effect, one recognizes that the mechanical power $r \times \Delta x$ applied to the bond approaches the power achieved by thermal fluctuations: $r \times \Delta x \approx \nu_{\text{off}} \times k_{\text{B}}T$. This means that the duplex would have no more time to escape from the potential well by fluctuations, because the loading rate that is applied approaches the attempt frequency very closely. For situations in which the mechanical work eventually equals the entire depth of the well, $F \times \Delta x = \Delta G_{\text{off}}$, the potential model is no longer valid, because it requires the possibility of the duplex escaping from the well by fluctuations. At this point, a description based on continuums mechanics like that in the work by Lebrun and Lavery (14) would describe the experiment adequately. We therefore argue that the kinetic barrier observed in Fig. 5, *a* and *b*,

probably occurs when the mechanically forced separation of the strands is faster than the opening kinetics of the fluctuation bubbles, and so thermal contributions are becoming less important for unbinding. In other words, once force has accumulated in a DNA helix that was opened partially by thermal fluctuations, the closing reaction of the bubble will be stalled by the applied strain, and further extension of the bubble will proceed until the strands are separated. When the force-loading rate, however, is faster than the inherent opening rate, the remaining base pairs will be disrupted predominantly by mechanics. Accordingly, stretched conformations with intact base pairing (S-forms) (Fig. 9 *d*) become more important for the transition state than bubbles when a critical loading rate $r \sim 9 \times 10^5$ pN/s is exceeded. The fact that even biotin-streptavidin complexes are disrupted close to the position on the slide where the kinetic effect occurred corroborates the observation that much higher forces are accomplished in the loading rate regime after the kinetic effect (Fig. 8).

According to Lebrun and Lavery (14), 5′-5′ pulling results in more stable conformations than 3′-3′ pulling because of better base stacking in the narrow fiber structure. However, our study demonstrates that duplexes pulled at 3′-3′ are more stable than their 5′-5′ counterparts. This contradiction possibly could be solved by the use of a theoretical model that places more emphasis on electrostatic repulsion than the simple solvent counterion model used by Lebrun and Lavery (14), as they already have suggested. Then, interstrand electrostatic repulsion probably would destabilize 5′-5′ stretched conformations more than 3′-3′ stretched conformations, because the phosphate distances are much shorter in the narrow fiber model.

Our hypothesis is summarized in Fig. 9: a), At zero force, DNA is in B conformation except for the ends, where the duplex is constantly opened and closed (curved arrows) by thermal fluctuations. b), At moderate loading rates, the bubbles are rapidly extended by fluctuations because the closing reaction is hindered by the applied strain that keeps one strand at every duplex end in single-stranded conformation. c), At a critical loading rate, the strain is applied faster than the fluctuations, and significant deformation work occurs, which drives both duplexes into different stretched conformations.

Explaining kinetic unbinding barriers by explicit relaxation times or the frequency of fluctuations might be relevant for receptor-ligand interactions in general. Kinetic unbinding barriers have been reported first for biotin-avidin (9,23) and later for antigen-antibody complexes (8,23). A relation between temporal fluctuations characteristics and the external pulling rate might be suitable to explain those barriers as well. Much slower fluctuation kinetics than for DNA bubbles must be assumed, however, because the barriers for avidin are found at 10^2 and 10^4 pN/s.

Our results provide evidence that opening of short DNA duplexes is assisted by thermal fluctuations up to a loading rate of $\sim 9 \times 10^5$ pN/s when force is applied in parallel to the helix. Above that limit, molecular machines would have to apply much higher forces in the separation of the double-stranded DNA due to higher energy dissipation. Of course, 9×10^5 pN/s is a very high value that hardly ever could be accomplished even by the strongest molecular machines. When proteins are bound to the helix, however, presumably lower loading rates are required to convert DNA into a stretched and completely closed conformation, comparable to those in RecA recombination. Moreover, it is likely that application of force in 5′-5′ direction causes ''inwinding'', leading to a double-stranded DNA of smaller diameter, as suggested by Lebrun and Lavery (14) and Konrad and Bolonick (15). Although this mechanism will not result in opening of long DNA, the smaller diameter may be useful in situations where DNA must be pulled through a narrow pore.

CONCLUSIONS (SUMMARY)

Stretching of DNA under applied force is a well-investigated issue by scientists in regard to several subjects. Nevertheless, not all aspects are completely understood, and we have presented an essential new observation. The stretching of 30 bp DNA in a molecular balance revealed that, beyond a certain loading rate, the orientation of the strands becomes crucial. We have explained this behavior through the existence of two distinct kinetic regimes through which different unbinding pathways are passed. Due to the changes in conformation, our results demonstrate that the 3′-3′ loaded strand is more stable than the 5′-5′ loaded strand at high loading rates. The question of whether different pulling directions and loading rates will cause different effects when proteins are bound to the helix is one of the next subjects to be addressed by molecular balance experiments.

SUPPLEMENTARY MATERIAL

To view all of the supplemental files associated with this article, visit www.biophysj.org.

We thank Dieter Braun for hardware support; Hauke Clausen-Schaumann for helpful discussions; and Ferdinand Kuehner and Steffen Mihatsch for providing the software to analyze the measured velocity values. We thank Richard Lavery for the Protein Data Bank files of stretched DNA and Dominik Ho for simulations and reviewing the manuscript. This work was supported by the Deutsche Forschungsgemeinschaft.

REFERENCES

1. Prevost, C., and M. Takahashi. 2003. Geometry of the DNA strands within the RecA nucleofilament: role in homologous recombination. *Q. Rev. Biophys.* 36:429–453.
2. Gelles, J., and R. Landick. 1999. RNA polymerase as a molecular motor. *Cell.* 93:13–16.
3. Albrecht, C., K. Blank, M. Lalic-Multhaler, S. Hirler, T. Mai, I. Gilbert, S. Schiffmann, T. Bayer, H. Clausen-Schaumann, and H. E.

Gaub. 2003. DNA: a programmable force sensor. *Science*. 301: 367–370.

4. Albrecht, C., H. Clausen-Schaumann, and H. Gaub. 2006. Differential analysis of biomolecular rupture forces. *J. Phys. Condens. Matter*. 18:1–19.
5. Neuert, G., C. H. Albrecht, and H. E. Gaub. 2007. Predicting the rupture probabilities of molecular bonds in series. *Biophys. J*. 93:1215–1223.
6. Schwesinger, F., R. Ros, T. Strunz, D. Anselmetti, H. J. Guntherodt, A. Honegger, L. Jermutus, L. Tiefenauer, and A. Pluckthun. 2000. Unbinding forces of single antibody-antigen complexes correlate with their thermal dissociation rates. *Proc. Natl. Acad. Sci. USA*. 97:9972–9977.
7. Strunz, T., K. Oroszlan, R. Schafer, and H. J. Guntherodt. 1999. Dynamic force spectroscopy of single DNA molecules. *Proc. Natl. Acad. Sci. USA*. 96:11277–11282.
8. Berquand, A., N. Xia, D. G. Castner, B. H. Clare, N. L. Abbott, V. Dupres, Y. Adriaensen, and Y. F. Dufrene. 2005. Antigen binding forces of single antilysozyme Fv fragments explored by atomic force microscopy. *Langmuir*. 21:5517–5523.
9. Merkel, R., P. Nassoy, A. Leung, K. Ritchie, and E. Evans. 1999. Energy landscapes of receptor-ligand bonds explored with dynamic force spectroscopy. *Nature*. 397:50–53.
10. Florin, E. L., V. T. Moy, and H. E. Gaub. 1994. Adhesion forces between individual ligand-receptor pairs. *Science*. 264:415–417.
11. Smith, S. B., Y. Cui, and C. Bustamante. 1996. Overstretching B-DNA: the elastic response of individual double-stranded and single-stranded DNA molecules. *Science*. 271:795–799.
12. Rouzina, I., and V. A. Bloomfield. 2001. Force-induced melting of the DNA double helix 1. Thermodynamic analysis. *Biophys. J*. 80:882–893.
13. Harris, S. A., Z. A. Sands, and C. A. Laughton. 2005. Molecular dynamics simulations of duplex stretching reveal the importance of entropy in determining the biomechanical properties of DNA. *Biophys. J*. 88:1684–1691.
14. Lebrun, A., and R. Lavery. 1996. Modelling extreme stretching of DNA. *Nucleic Acids Res*. 24:2260–2267.
15. Konrad, M. W., and J. I. Bolonick. 1996. Molecular dynamics simulation of DNA stretching is consistent with the tension observed for extension and strand separation and predicts a novel ladder structure. *J. Am. Chem. Soc*. 118:10989–10994.
16. Leckband, D., and J. Israelachvili. 2001. Intermolecular forces in biology. *Q. Rev. Biophys*. 34:105–267.
17. Wiegand, G., K. Neumaier, and E. Sackmann. 1998. Microinterferometry: three-dimensional reconstruction of surface microtopography for thin-film and wetting studies by reflection interference contrast microscopy (RICM). *Appl. Opt*. 37:6892–6905.
18. Rädler, J., and E. Sackmann. 1993. Imaging optical thickness and separation distances of phospholipid vesicles at solid surfaces. *J. Phys. II France*. 3:727–748.
19. Friedsam, C., A. K. Wehle, F. Kühner, and H. E. Gaub. 2003. Dynamic single-molecule force spectroscopy: bond rupture analysis with variable spacer length. *J. Phys. Condens. Matter*. 15:S1709–S1723.
20. SantaLucia, J., Jr. 1998. A unified view of polymer, dumbbell, and oligonucleotide DNA nearest-neighbor thermodynamics. *Proc. Natl. Acad. Sci. USA*. 95:1460–1465.
21. Lang, M. J., P. M. Fordyce, A. M. Engh, K. C. Neuman, and S. M. Block. 2004. Simultaneous, coincident optical trapping and single-molecule fluorescence. *Nat. Methods*. 1:133–139.
22. Lavery, R., and A. Lebrun. 1999. Modelling DNA stretching for physics and biology. *Genetica*. 106:75–84.
23. Neuert, G., C. Albrecht, E. Pamir, and H. E. Gaub. 2006. Dynamic force spectroscopy of the digoxigenin-antibody complex. *FEBS Lett*. 580:505–509.
24. Altan-Bonnet, G., A. Libchaber, and O. Krichevsky. 2003. Bubble dynamics in double-stranded DNA. *Phys. Rev. Lett*. 90:138101.